IEEE Photonics Journal
An IEEE Photonics Society Publication

Open Access

Characterization and Optimization of Field of View in a Holographic Waveguide Display

Volume 9, Number 6, December 2017

Zhongwen Shen
Yuning Zhang
Yishi Weng
Xiaohua Li

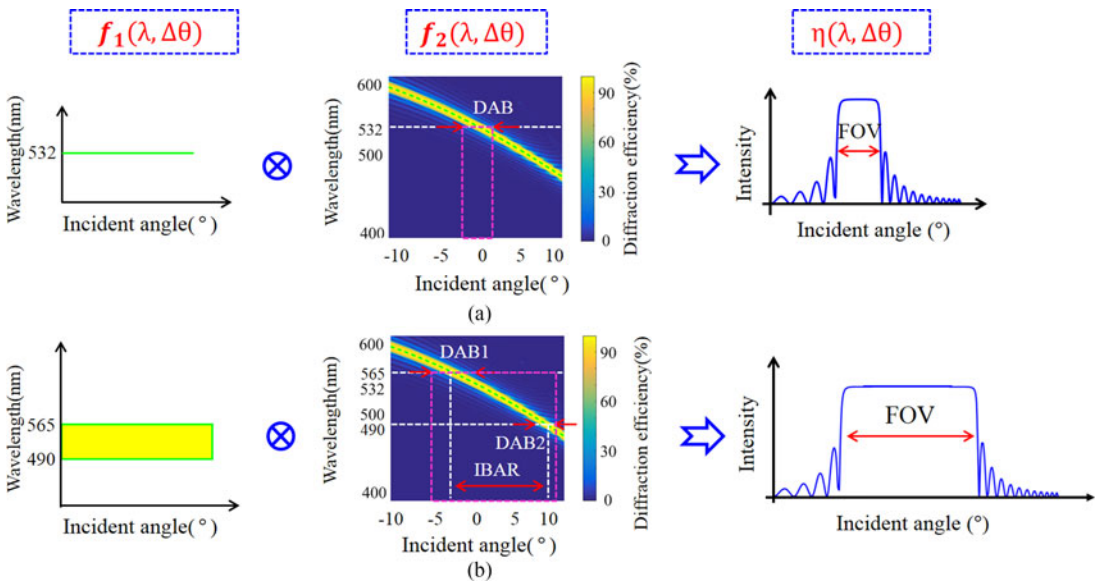

DOI: 10.1109/JPHOT.2017.2767606

Characterization and Optimization of Field of View in a Holographic Waveguide Display

Zhongwen Shen, Yuning Zhang, Yishi Weng, and Xiaohua Li

Joint International Research Laboratory of Information Display and Visualization, School of Electronic Science and Engineering, Southeast University, Nanjing 210096, China

DOI:10.1109/JPHOT.2017.2767606

Manuscript received September 26, 2017; accepted October 25, 2017. Date of publication October 30, 2017; date of current version November 14, 2017. This work was supported in part by the National Key Research Program under Grant 2016YFB0401201, in part by the Natural Science Foundation of China under Grant 61405033, and in part by the Natural Science Foundation of China under Grant 61505028.
Corresponding author: Y. Zhang (e-mail: zyn@seu.edu.cn).

Abstract: The paper presents the characterization of the field of view (FOV) in a holographic waveguide display (HWD) with a broadband spectrum image source. The influences of parameters such as grating slanted angle of volume holographic grating (VHG), grating period, and effective refractive index are systematically analyzed. We optimized the parameters and calculated the maximum FOV of monochromatic and chromatic HWD. A multilayered VHGs structure is proposed to enlarge the FOV effectively without additional cost and optical design. We also build a rigorous simulation model to verify the feasibility of the multilayered structure. The theoretical maximum FOV of monochromatic and chromatic HWD are presented after optimization.

Index Terms: Field of view, volume holographic grating, holographic waveguide display.

1. Introduction

The HWD technology is becoming widely used in the application of see-through devices. It involves the image source, the diffractive optical elements and the planar waveguide [1]. The VHGs are applied as the diffractive optical elements (DOEs) which steers the light with high angular and wavelength sensitivity [2]. It benefits from its light weight, small thickness and high ambient light transmittance [3], [4], but also suffer from the narrow operating angular range (i.e., narrow FOV) and severe chromatic dispersion in color display applications.

Before, the FOV for a HWD was principally discussed based on the single wavelength image source like a laser applied as the light source. So the FOV is directly related to the diffractive angular bandwidth (DAB) of the VHG. And the multiplexing VHGs configuration with different grating periods were proposed to widen the DAB [5], [6].

Nowadays, various kinds of micro-displays such as organic light emitting diode (OLED), liquid crystal on silicon (LCOS) with LED backlight can be served as the image source of HWD [7]. And these micro-displays usually have broadband spectrums rather than the single wavelength of a laser source. When the broadband spectrum micro-display is applied, the FOV depends on both the incident light spectrum and the DAB. Some researchers have mentioned the FOV for a broadband spectrum HWD [8]–[10]. However, as we know, the characterization of FOV performance in broadband spectrum HWDs has not been discussed systematically so far.

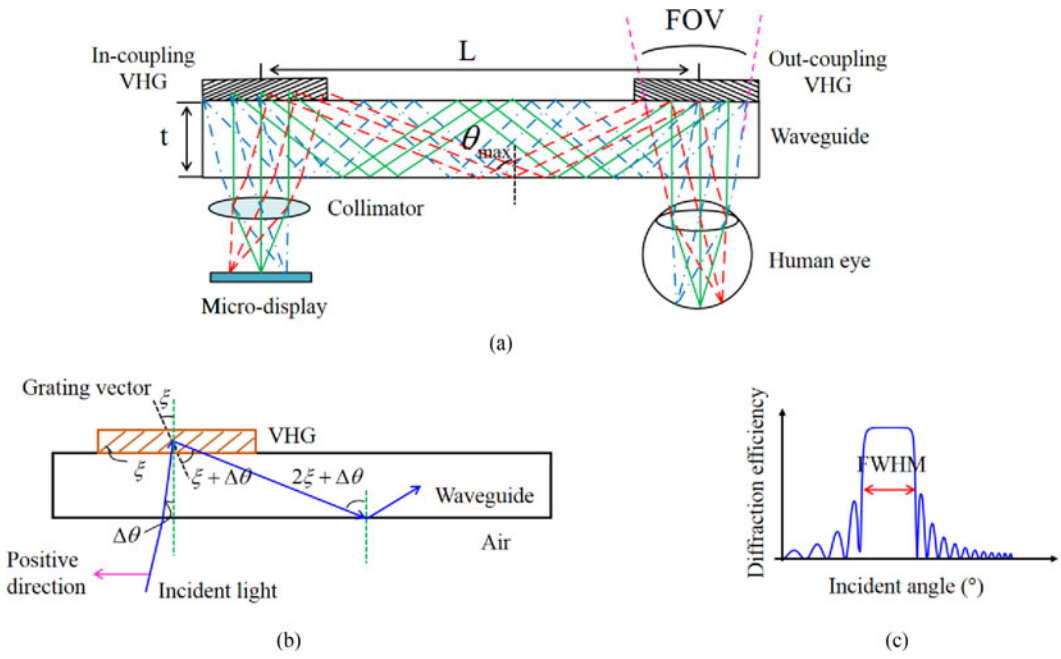

Fig. 1. (a) Basic configuration for a HWD. (b) Propagation mechanism of light beams in the waveguide. (c) Angular response of reflective VHG. FWHM is the full width at half maximum value of the angular response.

In this paper, the characterization of FOV in a broadband spectrum HWD is presented, considering the incident Bragg angle range (IBAR) and DAB. The refractive index of waveguide and parameters of a volume grating which include the slanted angle and period are studied to reveal the relativities between the FOV and these parameters. The optimized scheme is proposed to achieve the largest range of FOV by adjusting the above parameters. To further enlarge the FOV, a multilayered VHGs structure is applied and a rigorous simulation model based on the finite element method (FEM) is built to verify the performance of the design.

2. FOV Characterization

Fig. 1 shows the basic principle of a HWD [11]. The effective refractive index of a reflective VHG is designed same as that of the waveguide material. As a result of the collimation lens, light from different pixels will be collimated into different angles and incident onto the in-coupling VHG. The reflective VHG diffracts the incident light and makes the diffracted light beams propagate in the waveguide under the total inner reflection (TIR) condition. After propagation, the light beams exit the waveguide when diffracted by the out-coupling VHG which is normally placed as the mirrored symmetry with the in-coupling VHG. For a full-color display, the multilayered RGB VHGs could be used as the in-coupling and out-coupling optical elements. The images from the micro-display can be received by the eyes of the viewer [see Fig. 1(a)] when the collimated light is converged to different corresponding points on the retina [12]. The maximum angle range received by human eye indicates the FOV. However, for the traditional waveguide-based near-eye display system, the eyebox and exit pupil will decrease with the increase of the horizontal FOV. The exit pupil and eyebox of HWD can be effectively expanded by means of controlling the diffraction efficiency of the out-coupling VHG. The exit pupil magnification principle was studied before [13].

As shown in Fig. 1(b), Bragg diffraction occurs when the incident light entered the in-coupling VHG with corresponding wavelengths and angles. The propagating angle in the waveguide is $2\xi + \Delta\theta$. Here, ξ is the grating slanted angle of VHG refer to waveguide plane. $\Delta\theta$ represents the incident angle in the waveguide and it is zero for normal incidence. The propagating angle $2\xi + \Delta\theta$ should

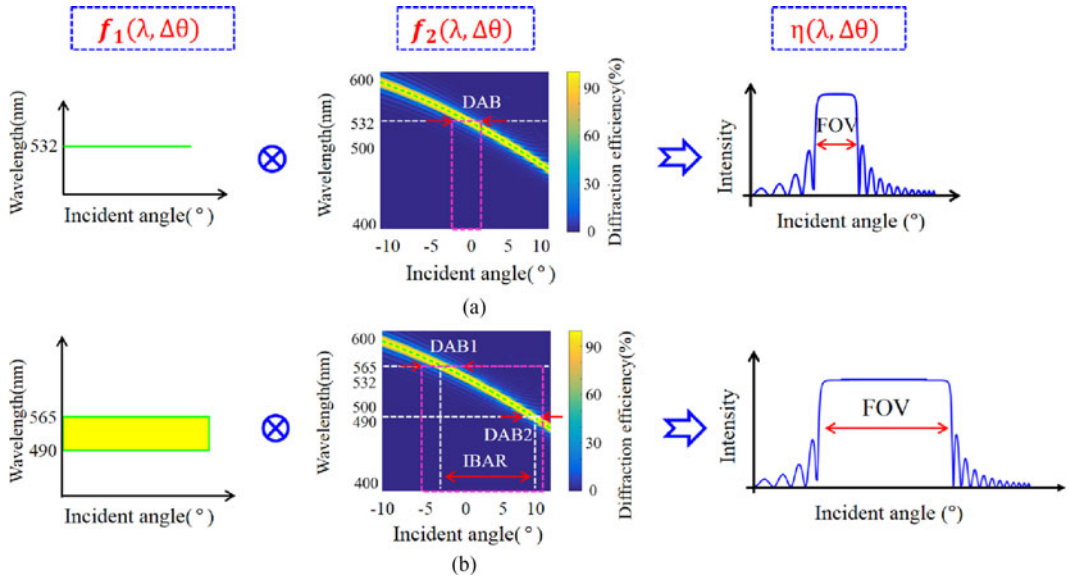

Fig. 2. Characterization of FOV considering two different micro-display sources. (a) FOV calculation when incident wavelength is 532 nm, (b) FOV calculation when incident wavelength varies from 490 nm to 565 nm.The incident angle range of pink dashed rectangular represents the FOV.

satisfy the TIR condition [14], that is,

$$\arcsin \frac{1}{n} \leq 2\xi + \Delta\theta \leq \theta_{\max} \tag{1}$$

The upper limit of propagation constraints $\theta_{\max}$ depends on the distance L between in-coupling and out-coupling VHGs and thickness t of the planar waveguide as shown in Fig. 1(a), which can be expressed by

$$\theta_{\max} = \arctan \frac{L}{2t} \tag{2}$$

In practical application, the eye box distribution should also be considered. Generally speaking, TIR angle over 80° with 2 mm thick waveguide creates very coarse eye-box distribution for individual field rays.

When the incident angles and the wavelengths match the Bragg condition, the diffractive efficiency can reach the peak value. However, if incident angle deviates from the Bragg angle in the certain wavelength, the diffraction efficiency will drop to zero rapidly according to Kogelnik's rigorous coupled wave theory [2]. As shown in Fig. 2(a), if a HWD uses the single wavelength light source with wavelength of 532 nm as an example, FOV equals to the DAB of the VHG directly. When the light illuminated from the micro-display has a wide spectrum as shown in Fig. 2(b). Both the incident light field function $f_1(\lambda, \Delta\theta)$ and diffraction function $f_2(\lambda, \Delta\theta)$ which is determined by VHG have common variables, so the output diffraction efficiency of HWD among viewing angle can be expressed by the following function:

$$\eta(\lambda, \Delta\theta) = f_1(\lambda, \Delta\theta) * f_2(\lambda, \Delta\theta) \tag{3}$$

Where $f_1(\lambda, \Delta\theta)$ is the micro-display spectrum in different incident angles, $f_2(\lambda, \Delta\theta)$ represents the angular response in the certain $\Delta\theta$ and λ.

As shown in Fig. 2(a) and (b), the incident wavelength λ and incident angle $\Delta\theta$ on the green dashed line in the figure of function $f_2(\lambda, \Delta\theta)$ satisfy the Bragg condition, the diffraction efficiency can always reach 100%. When the incident wavelength λ and incident angle $\Delta\theta$ are deviated from Bragg condition, the DAB can be calculated with the function $f_2(\lambda, \Delta\theta)$. And the IBAR can

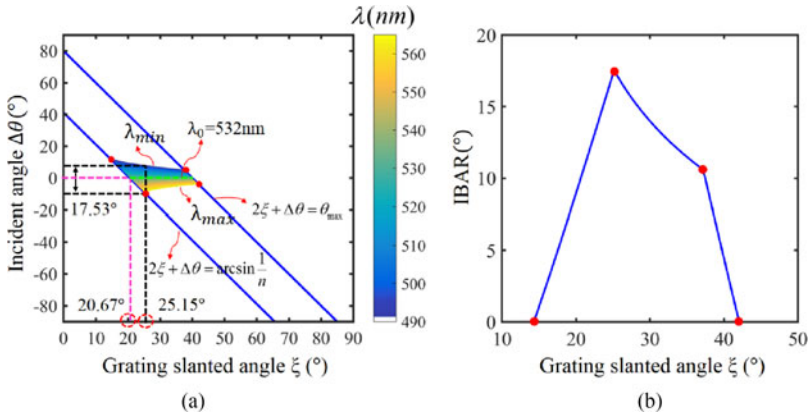

Fig. 3. (a) Bragg wavelength distribution considering propagation restrictions and incident wavelength range. (b) The IBAR when Bragg wavelength at 0° incidence of VHG is 532 nm, the effective refractive index is 1.52.

be calculated with the Bragg condition curve (green dashed line) if the micro-display spectrum is known. As shown in Fig. 2(b), the pink dashed rectangular represents the FOV of HWD with a broadband spectrum which can be calculated by three components: IBAR, DAB1 and DAB2.

As mentioned above, it's worth noting that the IBAR is also influenced by the propagation constraints in the waveguide. The effect of VHG parameters on the IBAR considering the propagation constraints will be discussed in detail below.

3. FOV in Monochrome HWD

3.1. Incident Bragg Angle Range (IBAR)

In the exposure process of reflection VHG, object light and reference light are interfered on the dry holographic plate from different sides of the plate [15].In this case, reference light is assumed to be perpendicular to the holographic plate, and object light is incident at a certain angle, which determines the grating slanted angle ξ. Interference fringes will be formed by the interference of reference light and object light in the photopolymer material. The grating period Λ (distance between the adjacent fringes) of reflection VHG is calculated by the following equations:

$$\Lambda = \frac{\lambda_0}{2n\cos\xi} \tag{4}$$

Where ξ is the grating slanted angle, λ_0 is the incident wavelength at 0° incidence, n is the effective refractive index of VHG. When incident light wavelength λ and incident angle $\Delta\theta$ satisfy the Bragg condition of reflective VHG, the theoretical diffraction efficiency can reach nearly 100%. This reconstruction process after exposure can be expressed by the Bragg equation:

$$\lambda = \frac{\lambda_0}{\cos\xi}\cos\theta_B = \frac{\lambda_0}{\cos\xi}\cos(\xi + \Delta\theta) \tag{5}$$

If incident light wavelength varies in the green wave spectrum (490 nm–565 nm) [16], the Bragg wavelength distribution of reflection VHG is calculated by the (5) as shown in Fig. 3(a). In Fig. 3(a), the green dashed line represents the Bragg wavelength at 0° incidence which is 532 nm. The effective refractive index of waveguide and VHG is 1.52. The blue solid straight lines $2\xi + \Delta\theta = \arcsin\frac{1}{n}$ and $2\xi + \Delta\theta = \theta_{\max}$ represent the boundary of propagation constraints from the (1). In Fig. 3, the maximum possible propagation angle $\theta_{\max}$ is 80°. The blue and yellow solid curves represent the Bragg wavelengths on the boundary of green visible spectrum. In Fig. 3(a), the IBAR firstly increases with the grating slanted angle ξ increases and finally reaches the maximum value 17.53° when $\xi = 25.15°$. After that, the IBAR decreases. Therefore, it is possible to find the best

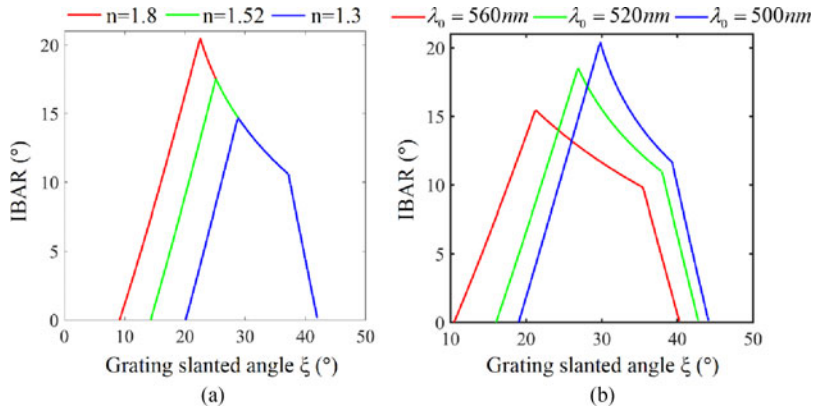

Fig. 4. (a) IBAR of reflection VHG with different refractive indexes. Bragg wavelength at 0° incidence of VHG is 532 nm. (b) IBAR of reflection VHG under different Bragg wavelengths at 0° incidence. The refractive index is 1.52. Incident light wavelength varies from 490 nm to 565 nm.

parameters of VHG and waveguide to realize the maximum IBAR. The Fig. 3(b) shows the detailed values of the IBAR in different grating slanted angles.

Fig. 4(a) shows the IBAR of VHG with three different refractive indexes. When refractive index is 1.3, the grating slanted angle ξ changes from 20° to 42°, the maximum IBAR is 14.72°. When refractive index is 1.52, the grating slanted angle ξ changes from 14° to 42°, the maximum IBAR is 17.53°. When refractive index is 1.8, the grating slanted angle ξ changes from 9° to 42°, the maximum IBAR is 20.5°. Therefore, with the increase of refractive index n, both of the grating slanted angle range and IBAR will become wider.

Fig. 4(b) shows the IBAR of VHG under different λ_0. The refractive index in Fig. 4(b) is set as 1.52 and the λ_0 (Bragg wavelength at 0° incidence) is 560 nm, the possible grating slanted angles ξ changes from 10° to 40°. If the grating slanted angle ξ is 21.35°, the maximum IBAR in the waveguide can reach 15.42°. When the Bragg wavelength at 0° incidence is 520 nm, grating slanted angle ξ is in the range of 16° to 42.5°, if grating slanted angle is 26.98°, the maximum IBAR in the waveguide is 18.42°. When the Bragg wavelength at 0° incidence is 500 nm, grating slanted angle varies in the range of 19° to 44°, and the maximum IBAR 20.42° is reached as the grating slanted angle is 29.81°. Therefore, the grating slanted angle range rises with the increase of Bragg wavelength at 0° incidence, but the maximum IBAR in the waveguide will be reduced on the contrary.

3.2. Optimum for VHG Parameters

Based on the above discussion of grating parameters effect on the IBAR, we can design the grating parameters (the effective refractive index n, grating slanted angle ξ, and grating period Λ) to optimize the IBAR. As shown in Fig. 5(a), after optimization, Bragg wavelength at 0° incidence is 534 nm, grating slanted angle ξ is 24.9°, grating period is 193.7 nm, the effective refractive index n is 1.52 and the maximum IBAR can reach 17°. The changing trend of IBAR with the variation of grating slanted angle is shown in Fig. 5(b). To fabricate the optimized VHG, we should calculate the incident angle of object and reference beams when using 532 nm solid laser. The calculation method has been introduced in detail before [17].

FOV in HWD is not only related to the IBAR but also involves the DAB of the corresponding Bragg wavelength at a certain incident angle as shown in Fig. 2(b). Based on the optimized grating parameters, the corresponding DAB of Bragg wavelength at incident angle $-8.5°$ and 8.5° in waveguide ($n = 1.52$). When light is incident at 8.5°, corresponding Bragg wavelength is 490 nm, the DAB is only 3°, as shown in Fig. 6(a). However, when light is incident at $-8.5°$, corresponding Bragg wavelength is 565 nm, the DAB is 8°, as shown in Fig. 6(b). According to Section 2, FOV in HWD can be calculated by the IBAR, DAB1 and DAB2. However, when incident angle $\xi\theta$ is $-8.5°$

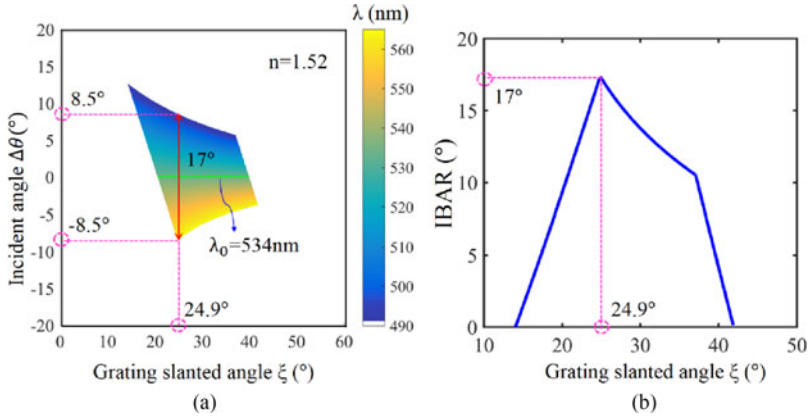

Fig. 5. (a) Optimized Bragg wavelength distribution, the effective refractive index is 1.52, Bragg wavelength at 0° incidence is 534 nm; (b) Optimized IBAR in the waveguide.

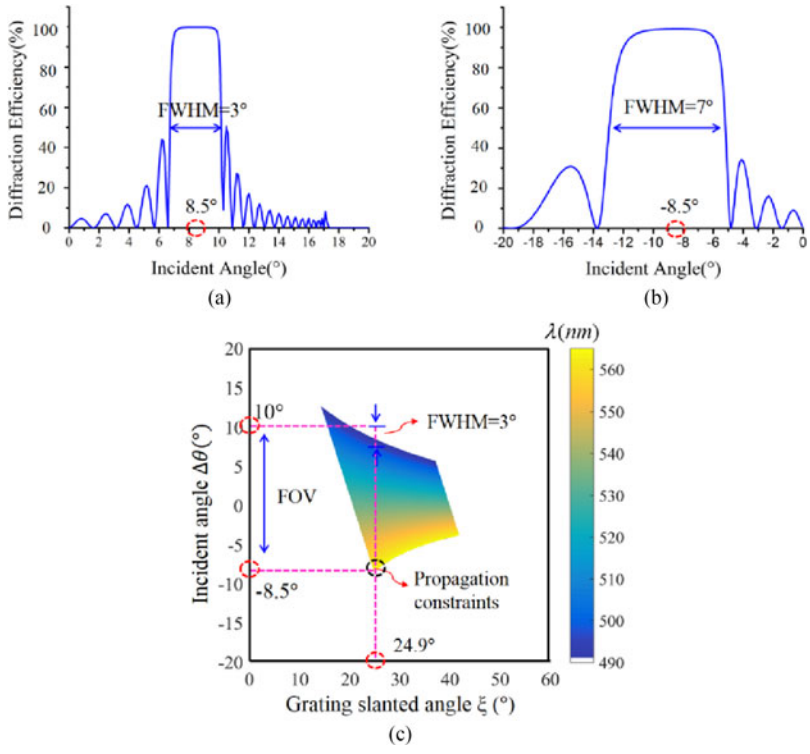

Fig. 6. (a) DAB2 at 8.5° incident angle; (b) DAB1 at −8.5° incident angle; (c) FOV considering DAB2 in the incident angle range. The refractive index modulation of VHG is 0.05, thickness is 10 μm, and grating slanted angle is 24.9°.

and the grating slanted angle ξ is 24.9°, the propagation angle $2\xi + \Delta\theta$ in the waveguide is equal to the TIR angle 41°. In order to ensure the propagation angle is greater than the TIR angle, the DAB when incident angle is −8.5° should be ignored. As a result, the FOV in HWD with optimized parameters can be enlarged to 18.5° in the waveguide, 28.3° in air. Based on the above analysis, the theoretical maximum FOV can be calculated by the following equation:

$$FOV = IBAR + \frac{DAB2}{2} \tag{6}$$

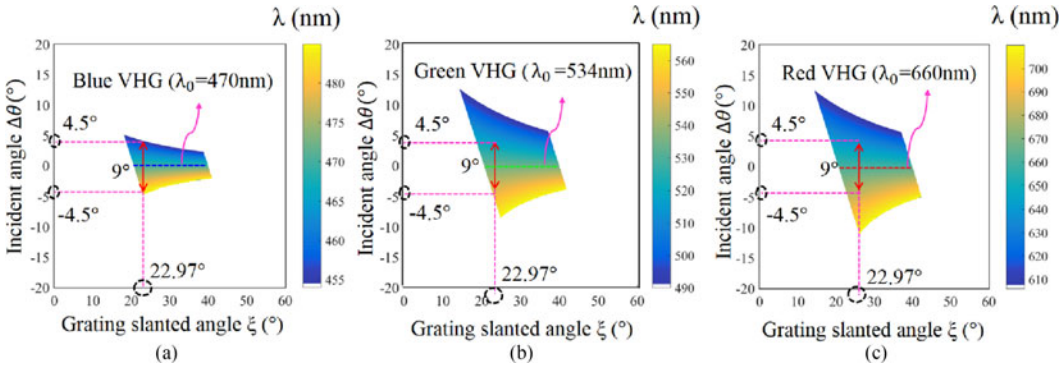

Fig. 7. Bragg wavelength distribution of RGB VHGs. Bragg wavelength at 0° incidence of RGB VHGs is (a) 470 nm, (b) 534 nm and (c) 660 nm, respectively. Refractive index of VHG and waveguide is 1.52.

4. FOV in Chromatic HWD

This paper adopts a multilayered RGB VHGs waveguide structure to realize color display. The thickness of single RGB VHGs is 10 μm, while waveguide thickness is 2 mm, so the thickness of multilayers VHGs can be ignored. The restrictions of incident light should be consistent with that listed in Section 2. Assuming that wavelength ranges of incident light are RGB visible light wave band, which are 606 nm–710 nm, 490 nm–565 nm and 454 nm–485 nm, respectively [16]. Fig. 7 shows the Bragg wavelength distribution of RGB multilayered VHGs. Changing the Bragg wavelength at 0° incidence of RGB VHGs can shift the Bragg wavelength distribution in the incident angle range. To realize colorful display in the whole FOV, the RGB IBARs should remain the same region as large as possible, as shown in Fig. 7. The refractive index of RGB VHGs is 1.52, the Bragg wavelength at 0° incidence of RGB VHGs is 660 nm, 534 nm and 470 nm. Therein, blue VHG has the narrowest IBAR, which is about 9°, as shown in Fig. 7(a). So the IBAR of blue VHGs determines the RGB IBARs. We mainly discussed influences of blue VHG parameters on the IBAR in the next section.

4.1. Optimum for VHG Parameters

The IBAR of blue VHG with different refractive indexes is shown in Fig. 8(a). When the refractive index increases, the possible range of grating slanted angle becomes wider, the maximum IBAR also increases. As shown in Fig. 8(b), the possible range of grating slanted angle increases with the Bragg wavelength at 0° incidence, on the contrary, the maximum IBAR decreases.

4.2. Diffractive Angular Bandwidth (DAB)

As shown in Fig. 7, the IBAR of RGB multilayered VHGs is from $-4.5°$ to 4.5°, but the DAB of Bragg wavelength on the IBAR boundary must be considered to calculate the FOV. Fig. 9 shows the DAB on the boundary of blue IBAR. As mentioned before, the DAB can become wider when the incident light is closer to the grating vector. When light is incident in $-4.5°$, the DAB of blue VHG reaches the peak values. On the contrary, when incident angle is 4.5°, the DAB of blue VHG will decrease to 4°. Considering the DAB of blue VHG and propagation constraints, FOV of chromatic HWD in the waveguide (n $=$ 1.52) is 11°, and can reach 16.8° in air.

5. Multilayered VHGs Design for FOV Enlargement

5.1. In a Monochromatic HWD

FOV of single green VHG waveguide structure (28.3°) is too narrow to satisfy the demand of customer. On the analysis of the IBAR of monochrome VHG, we find that changing the Bragg wavelength at 0° incidence can alter the IBAR and shift the location of IBAR. Therefore, we designed

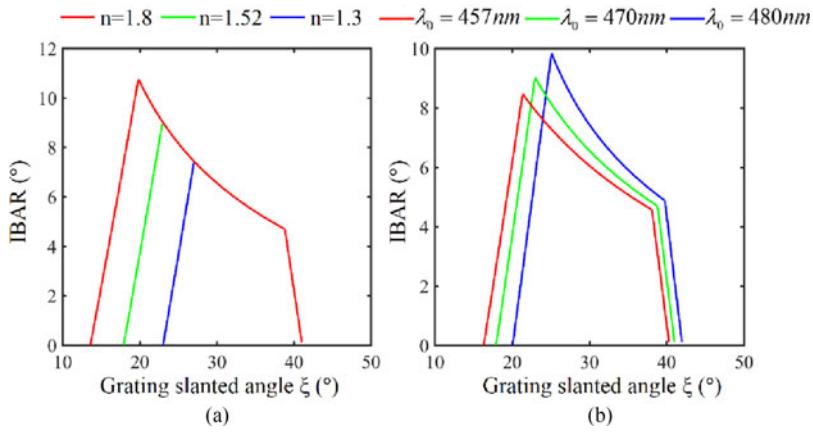

Fig. 8. (a) The IBAR with the variation of refractive index, Bragg wavelength at 0° incidence is 470 nm; (b) The IBAR with the variation of Bragg wavelength at 0° incidence when refractive index is 1.52.

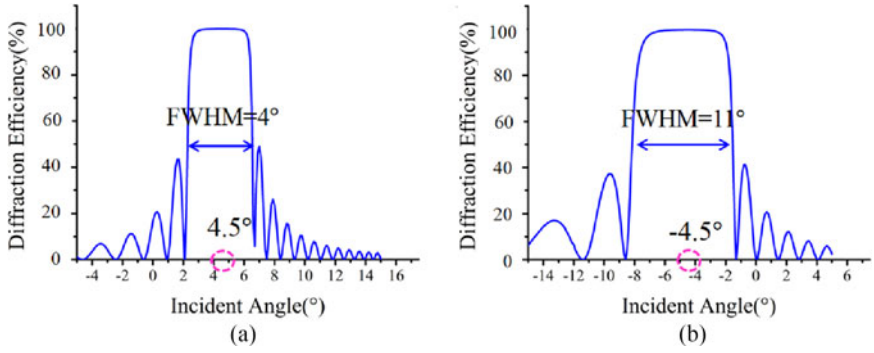

Fig. 9. DAB1 and DAB2 of blue VHGs. Grating slanted angle of RGB VHGs is 22.97°. (a) Bragg wavelength at 0° incidence is 470 nm, incident angle is 4.5°; (b) Bragg wavelength at 0° incidence is 470 nm, incident angle is −4.5°.

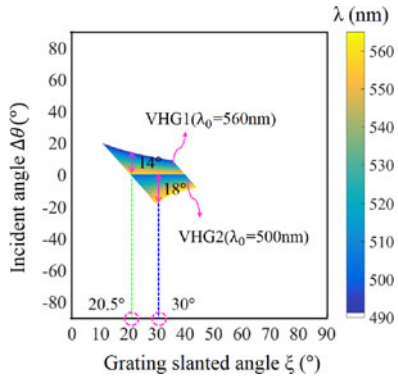

Fig. 10. Bragg wavelength distribution of VHG1 and VHG2. Bragg wavelength at 0° incidence of VHG1 and VHG2 is 560 nm and 500 nm. Incident wavelength range is from 490 nm to 565 nm.

a multilayered VHGs structure, as shown in Fig. 10. The Bragg wavelength at 0° incidence of two green VHGs is 500 nm and 560 nm, respectively, the Bragg wavelength distribution region of VHG1 just connects with that of VHG2. Light with positive incident angle only can be diffracted by VHG1, and VHG2 diffracts the negative incident angle range of the structure. The IBAR can be enlarged effectively by this method. When grating slanted angles of two VHGs are 20.5° and 30°,

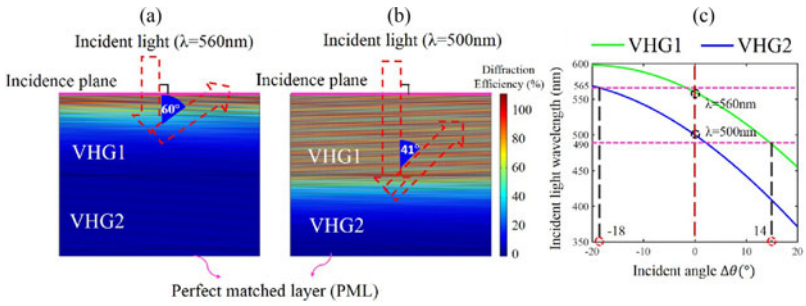

Fig. 11. Rigorous model of green multilayered VHGs structure based on FEM. (a) Bragg wavelength at 0° incidence of VHG1 is 560 nm; (b) Bragg wavelength at 0° incidence of VHG2 is 500 nm. In the model, refractive index modulation is 0.05. The thickness of two VHGs is 10 μm. The effective refractive index is 1.52. Red arrow represents the incident and diffractive directions of light beams. (c) Bragg wavelength curve of VHG1 and VHG2.

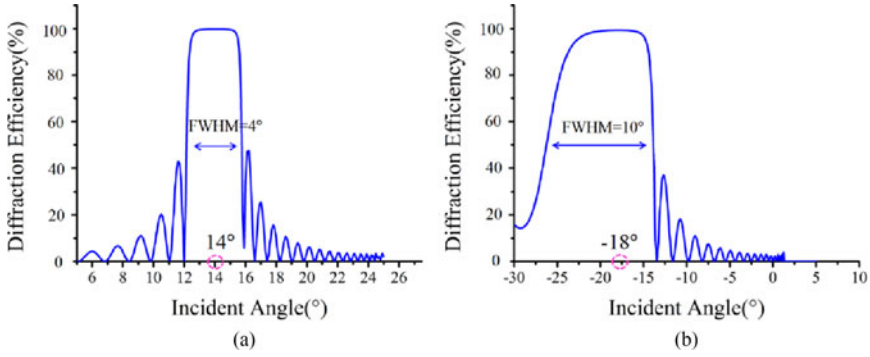

Fig. 12. (a) DAB2 at incident angle 14°; (b) DAB1 at incident angle −18°. The slanted angle of VHG1 and VHG2 is 20.5° and 30°. Grating thickness is 10 μm, the effective refractive index is 1.52, and refractive index modulation is 0.05.

the IBAR can reach the maximum value. To verify the performance, we built a simulation model of the multilayered VHG structure based on FEM.

According to the above analysis, the IBAR is related to Bragg wavelength distribution of VHG. As shown in Fig. 11(a) and (b) is the FEM model of green multilayered VHGs using COMSOL Multiphysics which is a commercial finite element package. The multilayered VHGs structure is illuminated by two light beams with two different wavelengths at normal incidence, respectively. In simulation, the grating period of VHG1 is 212.7 nm, VHG2's grating period is 175.6 nm. To ensure the maximum IBAR, the grating slanted angles of VHG1 and VHG2 are 20.5° and 30°. The results shown in Fig. 11(a) and (b) is only one example, because Bragg diffraction always occurs if only the incident angle and wavelength satisfy the Bragg condition. All cases between incident angle and wavelength which satisfy the Bragg condition of VHG1 and VHG2 are shown in Fig. 11(c). Pink dashed lines in the figure represent the boundary of green visible light wave band. It is easy to find that maximum IBAR can reach 32°.

Fig. 12 is the DAB when the incident angles are 14° and −18°, the incident wavelengths are 490 nm and 565 nm. The DAB is 4° when incident angle is 14°, and 10° when incident angle is −18°. However, the DAB at the negative incident angle should be ignored because of the TIR condition, so FOV of green multilayered VHGs in the waveguide (n = 1.52) can reach 34°, and 52.8° in air.

5.2. In a Chromatic HWD

As mentioned above, the IBAR of blue VHG limits the IBAR of RGB multilayered VHGs. As a result, in order to enlarge color FOV, we need to extend the IBAR of blue VHG as shown in Fig. 13(a),

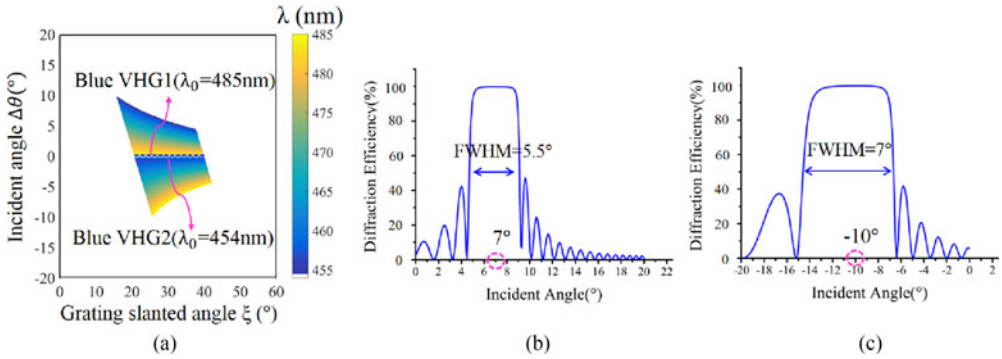

Fig. 13. Bragg wavelength distribution and the DAB of blue multilayered VHGs. (a) Bragg wavelength at 0° incidence of two blue VHGs is 454 nm and 485 nm, respectively; (b) The DAB2 when Bragg wavelength at 0° incidence is 485 nm, incident angle is 7°; (c) The DAB1 when Bragg wavelength at 0° incidence is 454 nm, incident angle is −10°.The effective refractive index is 1.52. Incident wavelength of blue light varies from 454 nm to 485 nm. Grating slanted angle of blue VHG1 is 25.6°, and grating slanted angle of blue VHG2 is 20.5°.

the expanded blue IBAR is composed of the IBARs under two different Bragg wavelengths at 0° incidence ($\lambda_{0B1} = 454$ nm, $\lambda_{0B2} = 485$ nm). When grating slanted angles of blue VHG1 and VHG2 are 25.6° and 20.5°, the incident angle can vary from −10° to 7°, which is included in the IBAR of red and green VHGs. The IBAR of red and green VHGs can be found in Fig. 7(b) and (c).

In order to match the blue IBAR, it is necessary to select appropriate grating slanted angles of green and red VHGs. The grating slanted angles of red and green VHGs should be consistent with that of the blue VHG2, so that the extended blue IBAR is among the IBAR of green and red VHGs. So the grating slanted angle of blue VHG2, green VHG and red VHG is 25.6°, and grating slanted angle of blue VHG1 is 20.5°.

Compared to the original single-layered VHGs, the multilayered structure can enlarge the IBAR by 8°, which reaches 17° (−10° to 7°). As mentioned before, the calculation of color FOV in HWD also needs considering the corresponding DAB2 of VHG on the boundary of the IBAR, as shown in Fig. 13(b) and (c). After the calculation of the IBAR and DAB2, as well as considering the propagation constraints, the actual FOV can reach 19.25° in the waveguide (n = 1.52) and 29.4° in air.

6. Conclusion

This paper characterizes the FOV in a monochromatic and chromatic HWD with broadband spectrum image source. The influences of grating parameters such as Bragg wavelength at 0° incidence, grating slanted angle, grating period and the effective refractive index on the IBAR are discussed. We build a rigorous model based on FEM to analyze the diffraction property of VHG, including the diffraction efficiency and DAB. The possible maximum FOV in both monochromatic and chromatic HWDs are 28.3° and 16.8° in air, considering the propagation constraints and the DAB. Then we propose a simple multilayered VHGs structure for enlarging FOV further. After optimization, the theoretical maximum monochromatic and chromatic horizontal FOV can be extended to 52.8° and 29.4° in air. This work presents the numerical analysis of FOV in HWD, which provides essential theoretical guidelines for the design of near-eye waveguide display system.

References

[1] H. Li, X. Zhang, G. W. Shi, H. M. Qu, Y. X. Wu, and J. P. Zhang, "Review and analysis of avionic helmet-mounted displays," *Opt. Eng.*, vol. 52, no. 11, 2013, Art. no. 110901.
[2] H. Kogelnik, "Coupled wave theory for thick hologram grating," *Bell Labs Tech. J.*, vol. 48, no. 9, pp. 2909–2947, 1969.
[3] A. Cameron, "Optical waveguide technology & its application in head mounted displays," in *Proc. SPIE*, Baltimore, MD, USA, 2012, vol. 8383, Art. no. 83830E.

[4] B. Kress and T. Starner, "A review of head-mounted displays (HMD) technologies and applications for consumer electronics," in *Proc. SPIE*, Baltimore, MD, USA, 2013, vol. 8720, Art. no. 87200A.
[5] Y. S. Wu, C. P. Chen, L. Zhou, Y. Li, B. Yu, and H. Y. Jin, "Design of See-through near-eye displays for presbyopia," *Opt. Exp.*, vol. 25, no. 8, pp. 8937–8949, 2017.
[6] J. Han, J. Liu, Y. C. Yao, and Y. T. Wang, "Portable waveguide display system with a large field of view by integrating freeform elements and volume holograms," *Opt. Exp.*, vol. 23, no. 3, pp. 3534–3549, 2015.
[7] A. Cameron, "The application of holographic optical waveguide technology to the Q-Sight family of helmet mounted displays," in *Proc. SPIE*, Orlando, FL, USA, 2009, vol. 7326, Art. no. 73260H.
[8] M. Piao and N. Kim, "Achieving high levels of color uniformity and optical efficiency for a wedge-shaped waveguide head-mounted display using a photopolymer," *Appl. Opt.*, vol. 53, no. 10, pp. 2180–2186, 2014.
[9] M. Piao, S. Gil, and N. Kim, "Design of wide angle holographic waveguide monocular head-mounted display using photopolymer," in *Proc. SPIE*, San Francisco, CA, USA, 2015, vol. 9386, Art. no. 9386K.
[10] Y. S. Weng, Y. N. Zhang, and X. H. Li, "Study on the field of view properties for a holographic waveguide display system," in *Proc. SID Symp. Dig, Tech, Papers*, San Francisco, CA, USA, 2016, vol. 47, pp. 7–10.
[11] H. Mukawa *et al.*, "A full-color eyewear display using planar waveguides with reflection volume holograms," *J. Soc. Inf. Display*, vol. 17, no. 3, pp. 185–193, 2009.
[12] L. Zhou *et al.*, "See-through near-eye displays enabling vision correction," *Opt. Exp.*, vol. 25, no. 3, pp. 2130–2142, 2017.
[13] L. Eison, M. Meykyar, M. Golub, A. A. Frisem, L. Gurwich, and V. Weiss, "Planar configuration for image projection," *Appl. Opt.*, vol. 45, no. 17, pp. 4005–4011, 2006.
[14] Y. Amitai, S. Reinhorn, and A. A. Frisem, "Visor-display design based on planar holographic optics," *Appl. Opt.*, vol. 34, no. 8, pp. 1352–1356, 1995.
[15] J. Piao, G. Li, M. Piao, and N. Kim, "Full color holographic optical element fabrication for waveguide-type head mounted display using photopolymer," *J. Opt. Soc. Koera*, vol. 17, no. 3, pp. 242–248, 2013.
[16] K. Kelly, "Color designations for lights," *J. Opt. Soc. Amer.*, vol. 33, no. 11, pp. 627–632, 1943.
[17] Z. M. Wu, J. Liu, and Y. T. Wang, "A high-efficiency holographic waveguide display system with a prism in-coupler," *J. Soc. Inf. Display*, vol. 21, no. 12, pp. 524–528, 2013.